Soft Matter

Sublimation of Isolated Toric Focal Conic Domain on Micro-Patterned Surfaces

Journal:	*Soft Matter*
Manuscript ID	SM-ART-12-2023-001678.R1
Article Type:	Paper
Date Submitted by the Author:	25-Jan-2024
Complete List of Authors:	Kim, Wantae; Korea Advanced Institute of Science and Technology, Chemistry Vitral, Eduardo; Rose Hulman Institute of Technology, Mechanical Engineering Leo, Perry; University of Minnesota, Aerospace Engineering and Mechanics Viñals, Jorge; University of Minnesota, school of physics and astronomy Kim, Dae Seok; Pukyong National University, Polymer engineering Yoon, Dong Ki; Korea Advanced Institute of Science and Technology, Department of Chemistry; KAIST, Graduate School of Nanoscience and Technology

ARTICLE

Received 00th January 20xx,

Accepted 00th January 20xx

DOI: 10.1039/x0xx00000x

Sublimation of Isolated Toric Focal Conic Domain on Micro-Patterned Surfaces

Wantae Kim[a]†, Eduardo Vitral[b]†, Perry H. Leo[c], Jorge Viñals[d]*, Dae Seok Kim[e]*, Dong Ki Yoon[a]*

Toric Focal Conic Domains (TFCDs) in smectic liquid crystals exhibit distinct topological characteristics, featuring torus-shaped molecular alignment patterns with rotational symmetry around a central core. TFCDs have attracted much interest due to their unique topological structures and properties, enabling not only fundamental studies but also potential applications in liquid crystal (LC)-based devices. Here, we investigated the precise spatial control of TFCDs arrangement using micropatterns and sublimation of TFCDs to estimate the energy states of the torus-like structures. Through simulations, we observed that the arrangement of TFCDs strongly depends on the shape of the topographies of underlying substrates. To accurately estimate the energetic effects of non-zero eccentricity and evaluate their thermodynamic stability, we propose a geometric model. Our findings provide valuable insights into the behavior of smectic LCs, offering opportunities for developing novel LC-based devices with precise control over their topological properties.

Introduction

Self-assembled structures, characterized by individual units that can form ordered patterns and mediate shape transitions, represent a fundamental concern across natural sciences, particularly within soft matter physics.[1-5] Notable instances of the intricate relationship between the molecular organization of a soft material and the resultant order, and orientation are evident from various morphologies in these systems. Examples of such soft materials include block copolymers,[6, 7] stacked membranes,[8-10] and various liquid crystals (LCs).[11-16] LC is a state of matter with intermediate properties between liquids and crystals. Of particular interest is the smectic phase of LC, characterized by its layered molecular ordering, in which these molecular layers preserve their equidistance.[17-22] Structures in the smectic A phase are characterized by the ordered arrangement of molecules normal to a layer, with long-range positional order within the layers but only short-range positional order between the layers.[23-26] One structural feature observed in the smectic A phase is the dimple-like defects, so-called toric focal conic domains (TFCDs).[15, 26-29] Due to the high elastic energy at the line defects around the core part of TFCDs, it is preferred to release energy by rearrangement of local directors near the line defects when the sample is perturbed. For example, when guest materials such as colloidal particles[13, 30] and reactive mesogens [31, 32] are introduced to TFCDs, they are trapped in the defect core. Furthermore, by manipulating the physically constrained space where TFCDs form, it is possible to control the hexagonal lattice arrangement of TFCDs since their density and arrangement are connected to the balance between the elastic energy and the surface anchoring energy at the boundaries.[27, 28, 33]

Recent intriguing results show that the sublimation of semi-fluorinated molecules in TFCDs at the smectic LC phase leads to the evolution of layering morphologies at micro- and nano-scales through molecules that leave and re-condense on the surface, which is different from previous studies that focused on manipulating and finding applications for the arrangements of TFCDs.[11, 15, 30, 34] Sublimation occurs from the LC surface while maintaining the internal layered structure, which is strongly influenced by the presence of semi-fluoroalkyl chains due to the specific charge balance.[35, 36] Despite the precise control achievable over the arrangements of TFCDs through the utilization of topographic patterns and applied electric fields,[37, 38] the investigation of TFCD sublimation has been limited to closely packed hexagonal arrays.[11, 15]

In this study, we investigate the sublimation of smectic LC layers in an isolated TFCD to provide a better understanding of the intricate interplay between elastic energy and surface anchoring. For this, various micro-patterned silicon substrates are employed, including channels, circles, and ellipses, so that diverse morphologies of TFCDs are investigated rather than the

[a] Department of Chemistry, Korea Advanced Institute of Science and Technology, Yuseong-gu, Daejeon 34141, Republic of Korea
[b] Department of Mechanical Engineering, Rose-Hulman Institute of Technology, 5500 Wabash Ave., Terre Haute, IN 47803, USA
[c] Department of Aerospace Engineering and Mechanics, University of Minnesota, 110 Union St. SE, Minneapolis, MN 55455, USA
[d] School of Physics and Astronomy, University of Minnesota, 116 Church St. SE, Minneapolis, MN 55455, USA
[e] Department of Polymer Engineering, Pukyong National University, Nam-gu, Busan 48513, Republic of Korea
† These authors contributed equally to this work.
Electronic Supplementary Information (ESI) available: [details of any supplementary information available should be included here]. See DOI: 10.1039/x0xx00000x

conventional hexagonal arrangement. Depending on the shape of the patterned substrate, sintering leads to a different evolution of the TFCDs via the sublimation and re-condensation of molecules, resulting in different morphologies. The experimental results obtained from direct observations agree with our theoretical analysis, elucidating the morphogenesis of sublimated TFCDs across a wide range of topographical shapes. We also contrast experimental observations with simulations based on a phase-field model for a smectic LC, which has previously reproduced transitions between TFCDs and morphologies such as conical pyramids during sintering. We believe our results can give insight into realizing a new soft matter design concept that utilizes sublimation and condensation to deliberately reshape and pattern unexplored structures.

Materials and Methods

Materials. All solvents were procured from commercial suppliers at reagent grade or higher purity. They were further purified to eliminate any residual moisture or oxygen. 3-Butenoic acid (97%), heptadecafluoro-n-octyl iodide (98%), tetrakis(triphenylphosphine)palladium (99%), lithium aluminium hydride (95%), ethyl 3-(4-hydroxyphenyl) benzoate (98%) were purchased from Sigma-Aldrich. Potassium carbonate (99%) was purchased from Alfa Aesar. Carbon tetrabromide (99%), triphenylphosphine(95%) were purchased from TCI Chemicals.

Synthesis of Y002. 5,5,6,6,7,7,8,8,9,9,10,10,11,11,12,12,12-heptadecafluoro-1-bromododecane reacted with ethyl 3-(4-hydroxyphenyl) benzoate, leading to the final synthesis of Ethyl 4′-[(5,5,6,6,7,7,8,8,9,9,10,10,11,11,12,12,12- heptadecafluorododecyl)oxy][1,1′-biphenyl]-4-carboxylate (Y002). The synthesized compound was purified through multiple extractions using water and dichloromethane, with detailed information in the Supplementary Information (SI).

Sublimation Procedure. The following detailed process was carried out to effectively interact with the Si substrate by adjusting the depth of the sample. The Si substrate was pretreated with 100 W UV irradiation to generate oxygen plasma, which resulted in a hydrophilic surface on the substrate. In the first step of the process, Y002 material is deposited on a Si substrate that has been heated to approximately 200 °C, which leads to an isotropic state. Upon cooling to around 190°C, TFCD forms randomly on the surface. The temperature is then maintained to allow slow sublimation to adjust the thickness. When the TFCD on the surface is observed under an optical microscope to begin being influenced by the pattern of the Si substrate, the substrate is reheated to 200°C to achieve an isotropic state (Figure 3a, i). Then, it is rapidly cooled at a rate of 5°C/min until it reaches a temperature of approximately 190-195°C. The sample undergoes a transition to the smectic A phase, and the formation of a uniformly distributed TFCD begins. Under the given conditions, arranging TFCD hexagonally is unfavorable, and the pattern of the underlying Si substrate strongly influences it. Afterward, the sample is rapidly cooled to 160°C (at 50°C/min) and annealed for approximately 40 minutes.

Characterization. Scanning electron microscope (SEM) samples were prepared by applying an osmium plasma coater to deposit a conductive osmium layer. Imaging procedures were carried out utilizing a Hitachi SU-8230.

Phase-Field Model and Computational Methodology. This work introduces simulations based on a weakly compressible model for smectic-isotropic interfaces, building upon previous phase-field models. The model describes a smectic phase in contact with an isotropic fluid, where each phase has a different density in LC molecules (e.g. a smectic interfacing a gas with small density of sublimated molecules). Numerical integration of the governing equations captures complex morphological transitions. It offers insights into how the alignment of layers and hemicylinders affect the interface thermodynamics and curvature-driven evolution, demonstrating relevance to experimental observations. The smectic is represented by a sinusoidal order parameter linked to modulations in molecular density across layers. The energy of the system accounts for displacement from planar layer configurations and deviations from equilibrium interlayer spacing, and densities. The energy density is expressed in terms of the order parameter and its derivatives. The model also presents a control parameter that sets if we have coexistence between phases or if one is energetically favored over the other.

The governing equations encompass mass, and momentum balances, and the smectic order parameter equation. These equations are numerically integrated using a pseudo-spectral method, with specific boundary conditions reflecting planar anchoring. Initial configurations present TFCDs under various conditions such as an isolated TFCD and a TFCD inside a channel. The surface tension and splay modulus can be written in terms of model parameters and are tied to each other through those. The simulations consider parameter settings in line with experimental data, ensuring a sensible ratio between splay modulus and surface tension. The chosen density penalization parameter remains small to account for heating effects and allows for sublimation. Viscosity constants, mobility, and equilibrium densities for both phases are specified.

Results

Sublimed Morphologies of Smectic TFCDs on Circular Pillars. Fig. 1a illustrates the chemical structure and phase transition

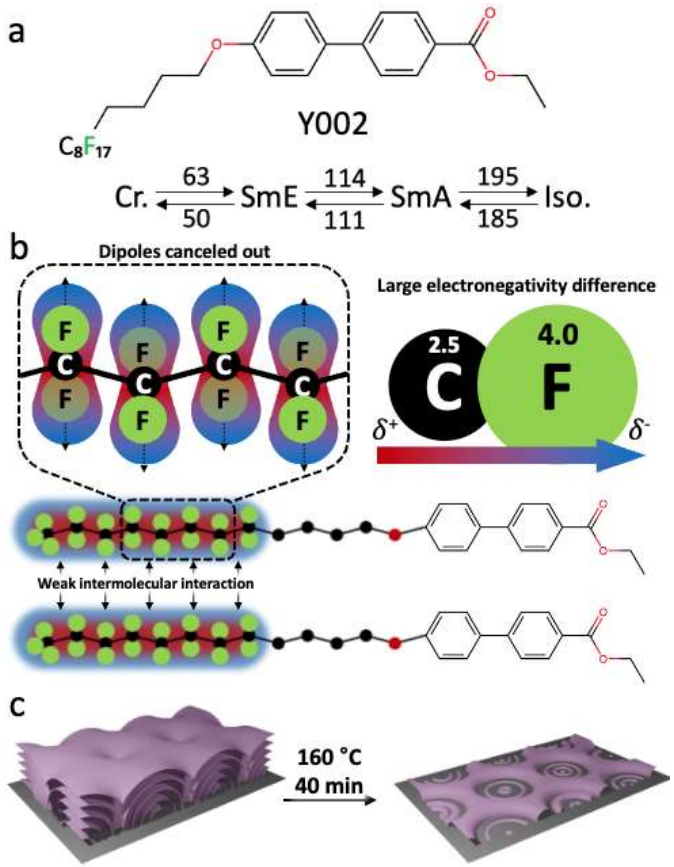

temperatures of Y002, a synthesized molecule with a perfluoroalkyl chain added to achieve its sublimation. Its unique properties have been studied in earlier research.[11, 15, 34] Y002 becomes an isotropic liquid state at temperatures above approximately 190 °C and a smectic A phase between 114 °C and 190 °C without passing through the nematic phase. In this phase, the molecules of a LC are arranged in layers or sheets parallel to one another. The layers are typically spaced apart by a distance roughly the same as the length of the LC molecule.[24, 39-41]

Figure 1. a) Molecular structure and phase transition temperature of Y002. b) Appearance of strong dipoles formed by the large electronegativity of fluorine. These cancel out and less intermolecular induced polarization occurs. c) Schematic images of the TFCD structure composed of Y002 of the SmA phase on flat Si substrate and the concentric circle pattern formed after sublimation.

Within the smectic A phase, a particular type of structure called the TFCD can arise. TFCDs are created in a smectic A phase when the LC molecules are placed between conflicting anchoring boundaries where one prefers planar anchoring, and the other prefers homeotropic anchoring. As a result, the smectic layers seek to form a tangentially bent layer stacking from one boundary to the other, forming a toroidal domain with a surface-frustrated singularity in which the director of LC molecules cannot be defined in three dimensions. The toroidal domains are closely packed and all connected with layering and a local director field in each domain forms two types of topological defects: one is a line defect at the core of TFCD, and the other is a circular defect at the bottom, schematically represented in Fig. S2a.[42-44] The smectic layers are illustrated with pink color on the left side of the image in Fig. 1c, with a noticeable indentation, called a "dimple", located at the center of the TFCD domain (see also the hexagonal arrays of dimples in Fig. S2b, S2c). The arrangement of TFCDs is typically hexagonal when deposited on a flat substrate; however, TFCDs exhibit different arrangements depending on the geometries of underlying substrates, such as channels and micro-posts.[28, 44-46] Arrays of TFCDs can be affected by a complex interplay between the elastic energy caused by the curvature of the LC layer and the surface energies of the air-LC and substrate-LC interfaces.

Interestingly, Y002 is a material that exhibits the property of sublimation, indicating the transition from the smectic A phase to a gas phase (typically, sublimation refers to the transition from a solid to a gas phase). This sublimation can be attributed to the presence of a perfluoroalkyl chain within the molecule (Fig. 1b). The strong electronegativity of fluorine in perfluoroalkyl chains causes symmetric arrangement of dipoles, hindering intermolecular interactions due to a strong electrical barrier and a lack of induced dipole formation, leading to minimal dispersion force influence.[15, 34, 45] This property is effective even in the crystalline state, where the molecules are tightly packed. Due to the low intermolecular forces, the molecules in the outermost layer tend to escape from the surface with thermal stimuli, leading to sublimation. When TFCDs made of Y002 are thermally annealed at 160 °C on a flat silicone substrate or circular micro-post, an intriguing concentric semi-toroidal pattern is revealed within an hour (Fig. 1c, Fig. S3). Once the concentric hemicylindrical patterns form, they remain stable for over 90 minutes during the subsequent annealing process. The concentric hemicylindrical patterns appear to be associated with the internal organization of the TFCD assembly and exhibit a longer-lasting stability compared to the dimple structures. It is essential to perform an energy analysis of the changes occurring at the surface to analyze the distinctive structures formed from the sublimation process.

The surface curvature of the TFCD consisting of Y002 plays an essential role in describing the sublimation or evaporation rates. For this, a single TFCD is isolated from the TFCD film with micro-pillars substrate to observe a detail of curvature-evolution in the TFCD. A detailed investigation has been conducted on the sublimation processes of Y002 on a Si substrate with micro-pillars to enhance our comprehension of TFCDs and their stability. The sublimation of the TFCD array on the Si substrate with micro-pillars was carried out by precisely controlling the depth of pillars in a range of from 2 to 3 μm (Fig. 2a). Initially, similar to previous literature,[28] TFCD cores are centered on circular pillars, with satellite TFCDs positioned between groups of four neighboring pillars (Fig. 2d). Subsequently, through thermal annealing at 160 ℃ for approximately 1 hour, concentric hemicylindrical patterns of Y002 formed on the pillars (Fig. 2b). While these patterns share similarities with those formed on a flat Si substrate, they are distinctly isolated within the pillars. While significant sublimation occurs around the pillar vicinity at depths

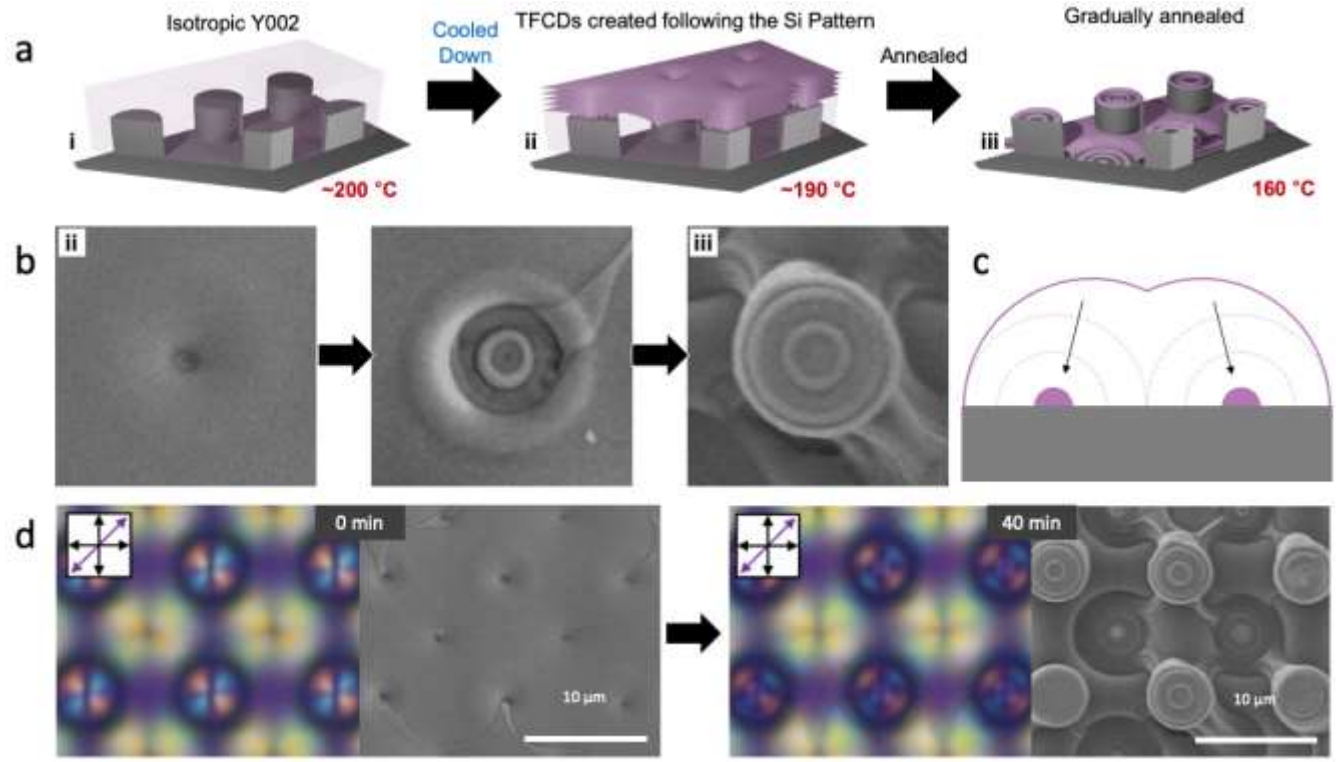

Figure 2. a) The sublimation process of Y002 on a Si pattern; i. The substrate is heated to 200 °C to achieve isotropic state. ii. When cooled at a rate of 5 °C/min, the arrangement of TFCDs is significantly influenced by the Si substrate pattern beneath the Y002 surface. iii. The TFCDs are annealed and fixed for less than an hour at 160°C. b) Top-view SEM images of sublimation process of Y002 in circular pillar patterns. c) Side-view schematic image of sublimation process of Y002 in circular pillar patterns. d) Sublimation process and schematic illustration of Y002 in circular pillar patterns array.

exceeding 5 μm, it's worth noting that the concentric patterns on top of the pillar largely remain intact. This result is similar to the previously observed retention of concentric patterns on the top of the square micro pillars pattern from TFCD film over the substrate.[34] The thermal stability of the evolved layering structures implies a lesser degree of sublimation from the concentric residue. This intriguing outcome emphasizes the complex interplay between the sublimation dynamics and the inherent structural characteristics of the TFCDs.

To better understand the sublimation process, the evolved topographies of the smectic layering were investigated through SEM images (Fig. 2). Initially, the sublimation occurs gradually, commencing from the highest layers on the film. Annealing occurs within a straightforward TFCD setup connected to its surroundings (as depicted in Fig. 2a, ii). Following its detachment from the surroundings (as shown in Fig. 2c), it assumes the form of a spindle torus. Subsequently, the droplet takes a circular shape until it reaches the core. Finally, it forms and isolates a circular residue onto the pillar, which occupies precisely half the diameter of its TFCD (Fig. 2b, c). As the sublimation progresses, it passes through a horn torus and becomes a ring torus (donut) shape. The bottom of the torus with the core layers corresponds to the central axis of the torus and remains the longest.

Surface Tension and Smectic Morphologies. Before we discuss the effect of changing the substrate geometry, it is important to talk about the implications of a low Bond and high Laplace numbers to the evolution of a smectic surface. When a simple solid crystal sublimates from the surface, the molecular orientations and arrangements remain fixed and are exposed. Factors such as the local stress and strain relationship cannot be applied. In contrast, when evaporation occurs on the surface of an isotropic liquid, the molecular orientations dynamically change due to the free-flowing nature of the fluid, resulting in the continuous relaxation of partial stresses in droplets.[47-50] As a result, the structural characteristics of the interface are spontaneously and continuously relieved.

LCs possess both crystalline order and fluidic behavior. Therefore, liquid-like physical properties such as surface tension and viscosity still apply. Ultimately, Y002 is a crystalline fluid in the smectic phase, where structural loss occurs from the surface down to the layer level. It exhibits clear distinctions from the sublimation of simple solid crystals or the evaporation of isotropic liquids. The real-time morphological changes due to the surface tension during the sublimation process can be explained by the Bond number (*Bo*) of the fluid [51]

$$Bo = \frac{\rho g L^2}{\gamma}$$

where ρ is the density, g is gravitational acceleration 9.8 m/s², L is the characteristic length, like the radius of curvature for a droplet, and γ is the surface tension. The Bond number is dimensionless, representing the importance of surface tension in a fluid system. When the Bond number is small ($Bo \ll 1$), surface tension dominates and has a pronounced effect on the surface morphology. On the other hand, when the Bond

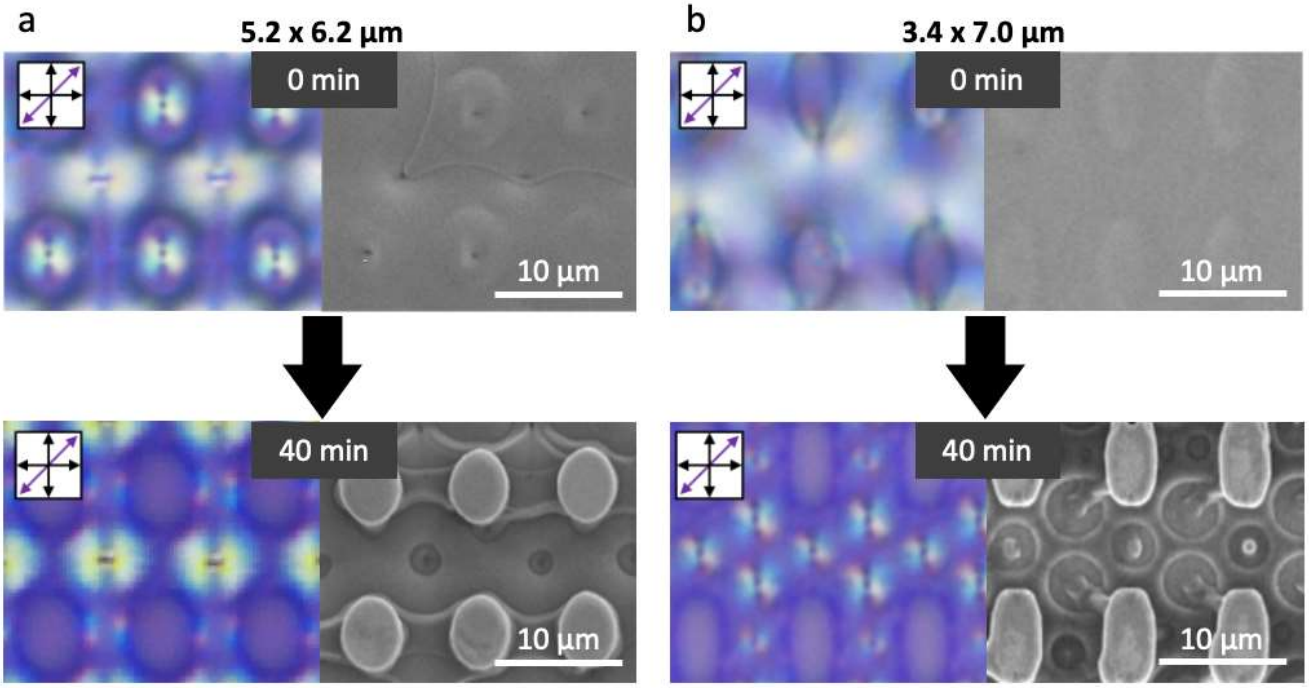

Figure 3. Sublimation process of Y002 in two elliptical pillar patterns. a) 5.2 x 6.2 µm, and b) 3.4 x 7.0 µm.

number is large (*Bo* >> 1), gravity becomes more significant, leading to different fluid behaviors. With a reference droplet size of 5.5 µm, Y002 exhibits a Bond number in the range of 10^{-5}. This signifies that the influence of surface tension is pronounced enough to remain largely unaffected by gravitational forces, directly impacting the surface morphology. However, it exhibits distinct characteristics compared to the evaporation of a simple isotropic liquid droplet.

Due to its high viscosity, Y002 experiences significantly limited flow within the system, resulting in restricted movement and deformation of the droplet. As a result, the stress induced by the droplet deformation remains prominent, and this is evident in the changes observed during the sublimation process. Meanwhile, as the outermost surface molecules are not firmly fixed, surface tension may impact the interface structure of droplets formed after sublimation. The Laplace number (*La*) is a dimensionless number that also represents the relative importance of viscous forces to surface tension forces in a fluid system. It provides a numerical measure of behavior differences between LC and isotropic liquids. It is defined as:

$$La = \frac{Re^2}{We} = \frac{\rho\gamma L}{\mu^2} = \frac{\text{inertia} \cdot \text{surface tension}}{\text{viscous forces}^2}$$

where μ is the viscosity, Reynolds number (Re) is a dimensionless number that represents the relative importance of inertia and viscosity in a fluid flow, and it determines the flow characteristics of the fluid. Weber number (We) is a dimensionless number that quantifies the relative importance of inertial forces to surface tension forces in a fluid system, providing insights into the behavior of fluid flows and the deformation of fluid interfaces. A large Laplace number signifies a significant ratio between surface tension and momentum transport within a fluid. The maintenance of fine droplet structures under conditions such as atomization is primarily characterized by a high the Laplace number.[52-54] It indicates that the influence of surface tension forces is relatively strong compared to the fluid's momentum, affecting the behavior and dynamics of fluid interfaces, as in the case of the smectic A surface.

Sublimed Morphologies of Smectic TFCDs on Elliptical Pillars. In contrast to circular pillars, experiments using a non-circular elliptical pillar pattern yielded significantly different results. (Fig. 3) When the TFCDs were positioned on an ellipse with an eccentricity of 0.573 (Fig. 3b, left), their depth on the Y002 surface was comparatively shallower than in the case of a circular pattern. During sublimation, irregular concentric residues resembling the TFCD structure formed temporarily. These residues sublimated and disappeared relatively quickly. (Fig. S6) On the other hand, for an elliptical pillar with a larger eccentricity of 0.807 (Fig. 4b, right), achieving precise positioning of the TFCDs at the center proved considerably challenging. The resulting residue exhibited an irregular shape and tended to sublime rapidly, eventually vanishing completely. This finding suggests that the highly deformed smectic A layer structure becomes notably unstable. The observed instability is attributed to the asymmetric deformation when the smectic A layer forms TFCDs. In particular, it is expected that significant splay deformation occurs at the point corresponding to the long axis of the ellipse.

The interface thermodynamics of fluids is highly sensitive to the geometric structure of such interface. In particular, the

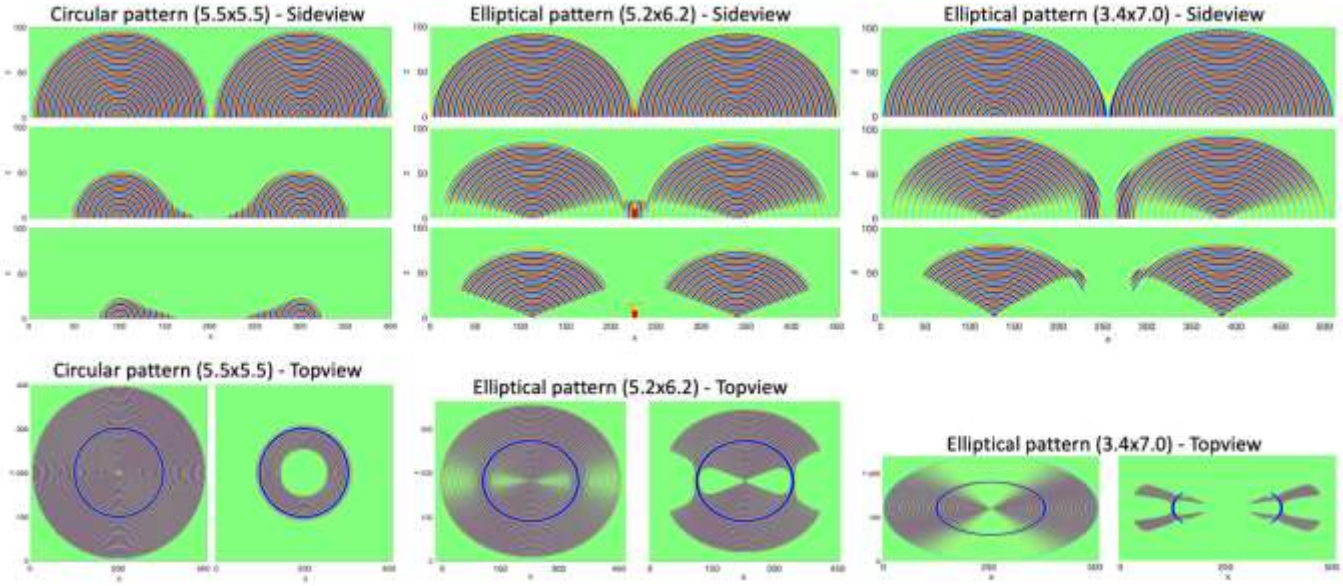

Figure 4. Simulation images of the TFCD droplet sublimation process, with an initial order parameter condition consisting of a half spindle torus with circular and elliptical bases. The blue and red lamellae represent the smectic layering, and the green is a distinct isotropic phase. The thick blue lines on top-views indicate the central circle of the torus.

influence of interface curvature on phase transitions is described by Kelvin's or Young-Laplace equation.[51, 55, 56] It describes the relationship between the change in equilibrium vapor pressure and the curvature of an interface. The Laplace pressure, the difference of vapor pressure across the interface, denoted as Δp, can be expressed as:

$$\Delta p = \gamma \nabla \cdot \mathbf{N}$$

where γ is the surface tension. The unit normal vector, $\mathbf{N}$, is perpendicular to a surface at a given point toward the outside. The term $\nabla \cdot \mathbf{N}$, representing the divergence of the unit normal vector, can be expressed in terms of curvature. It is equal to twice the mean curvature ($2H$), which is the sum of the reciprocals of the principal radii of curvature $\left(\frac{1}{r_1} + \frac{1}{r_2}\right)$.

In regions of high curvature, the Kelvin equation suggests an enhancement in the process of sublimation or vaporization, so that molecules have a stronger tendency to transition to the vapor phase. In the case of an elliptical droplet, the Kelvin equation tells us that there will be differences in vapor pressure along the azimuth angle of the ellipse (i.e. between regions of higher and lower curvature). This imbalance leads to asymmetric phase transitions, disrupting the stable TFCD structure formed by the smectic A phase. As a result, the system becomes more unstable when compared to the axially symmetric TFCDs on circular pillars. This phenomenon can be attributed to splay deformation, leading to increased thermodynamic activity caused by molecular instability. The splay deformation of molecules in the curved regions increases the intermolecular spacing, reducing the cohesive forces between the molecules. As a result, the molecules in the curved regions have higher thermal energy, leading to an increase in the vapor pressure of the droplet.

In the case of torus droplets arranged in a circular pattern, sublimation occurs more slowly in the inner region of the ring, which has a negative curvature component, which can also be observed from simulation results in Fig. 4. This corresponds to concentric circles remaining in the inner region of the ring, as seen at the half point during the actual sublimation process. Due to the appropriate fluidity of Y002 and its high surface tension, it reassembles into droplets and converges into a torus shape instead of a spherical shape. (Fig. S3) The residues formed near the dimples during the sublimation of TFCD arrays on a flat substrate are structurally and topologically equivalent to the concentric circular trace within the 1/2 ring of the circular pillar. (Fig. S5) If the droplet's crystallinity decreases and its ordering ability of molecules decreases, the torus droplet described earlier may not be maintained during the sublimation process. After the initial formation of the TFCD array, if the smectic phase is maintained at a high temperature of 190 °C and rapid sublimation occurs, a spherical droplet typically forms at the centers of the TFCDs, which are the dimple positions. However, this spherical droplet exists only for a very short period and quickly sublimates and disappears.[15] This is attributed to the decrease in crystallinity and reduction in surface tension of Y002 at high temperatures, coupled with a more significant decrease in viscosity.

Although the Kelvin equation provides a quantitative relationship between vapor pressure and droplet curvature, it assumes the liquid is isotropic and does not consider effects of molecular order in the droplet. Therefore, this equation is inadequate for explaining the complete evaporation dynamics of non-isotropic droplets, including those displaying intricate internal organization or crystallinity. The surface energy of the droplet is strongly influenced by the molecular ordering, and classic interface thermodynamics relations can even change to leading order in curvature depending on the molecular arrangement [58], which needs to be considered when modeling the evaporation of non-isotropic droplets. We will next look into the strain energy density of a LC, which does present a dependence on the director field and discuss how it

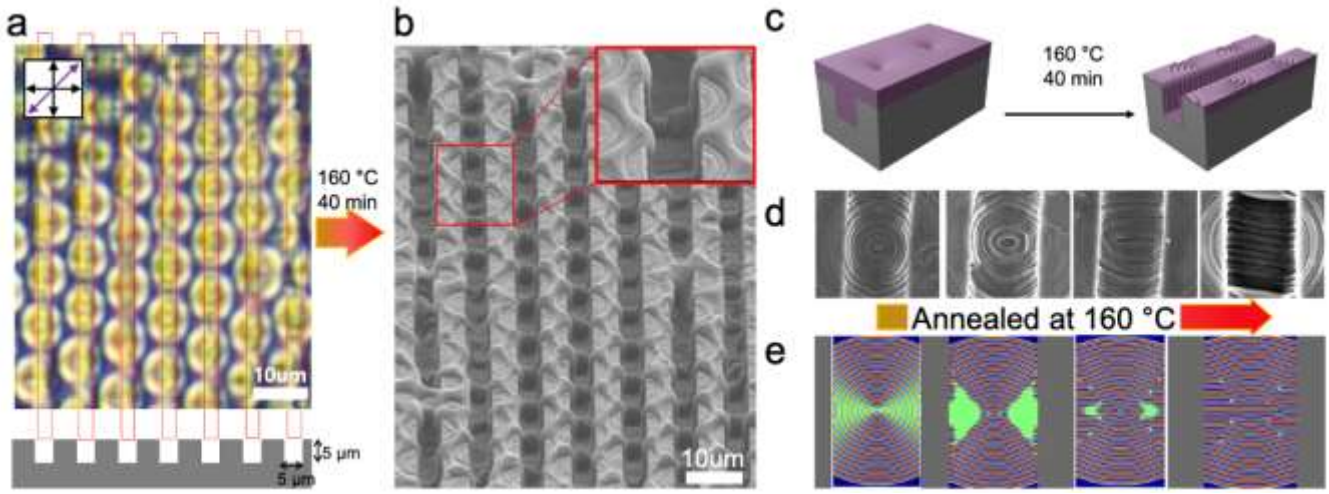

Figure 5. a) Polarized optical microscope (POM) and b) SEM images of sublimation process of TFCDs array on a 5 μm-channel patterned Si wafer. c) Schematic images of sublimation process of TFCDs array. d) Top view of SEM images of sublimation process of TFCDs array. e) Simulation comparisons corresponding to SEM images of each sublimation process.

can help us understand the behavior of smectic phases, including sublimation.

Energy Calculation. The residue patterns that emerge following the sublimation of TFCD droplets result from the sublimation of the smectic A liquid crystal (LC) phase. This non-uniform sublimation process preferentially directs the evaporation or sublimation along specific orientations, giving rise to distinct residue patterns on the surface. The sublimation rate significantly influences the formation of these residue patterns. The speed at which TFCD droplets undergo sublimation determines the time available for the remaining material to reorganize, and during this period, surface tension aids in facilitating this reorganization. Therefore, the ultimate residue patterns observed after TFCD droplet sublimation are determined by the interplay between the surface tension of the smectic A phase and the sublimation rate. These patterns offer valuable insights into the surface properties and dynamics of the LC system, contributing to a deeper understanding of the behavior of this complex material.

The elastic deformation energy of a smectic LC is a crucial factor in understanding its behavior and predicting its properties, which connects experimental observations to simulation results. For a nematic LC, the deformation energy that arises from distortions of the director field is described by the well-known Oseen-Frank elastic free energy. This energy functional presents contributions from the splay, twist, and bend deformation modes, which represent the energy cost of deforming the director field in different ways.

The total free energy density of a LC can be written as $F_T = F_0 + F_d$, where F_0 is the energy of the uniformly aligned molecular state and F_d is a distortion term. This is the Oseen-Frank free energy, given by the expression:

$$F_d = \frac{K_1}{2}(\nabla \cdot \mathbf{n})^2 + \frac{K_2}{2}(\mathbf{n} \cdot \nabla \times \mathbf{n})^2 + \frac{K_3}{2}|\mathbf{n} \times \nabla \times \mathbf{n}|^2$$

where **n** is the director field and K_1, K_2, and K_3 are the splay, twist, and bend elastic constants, respectively. For the smectic A, the twist and bend deformation modes of n are restricted, so that only the splay of molecules are allowed, which corresponds to bending of the smectic layers. Besides bending of layers, deviations from the equilibrium interlayer spacing also contribute to the smectic elastic energy, which are not included in this analysis. Since sublimation occurs at the outermost layers, there is no need to consider the interaction with the substrate. Therefore, the deformation energy density of the outermost layer of TFCD, considering the sublimation of torus-shaped droplets, can be abbreviated as follows:

$$F_d = \frac{K_1}{2}(\nabla \cdot \mathbf{n})^2.$$

If the director field is aligned with the surface normal **N**, as is the case of TFCD outer layers, then $\nabla \cdot \mathbf{n}$ becomes equivalent to the term that appears in the Kelvin equation, which is twice the mean curvature *H* of the TFCD surface. Therefore, regions of increased *H* in TFCDs on elliptical pillars will be less stable. This energy penalization is also present in the phase-field model we adopt, which presents model parameters that can be related to the elastic constant K_1.

Numerical Results. To further investigate the stability of TFCDs on substrates of different geometry, we will simulate the evolution of a TFCD during sintering based on a weakly compressible model for a smectic-isotropic interface[57], which builds on previous phase-field models[58, 59]. This is a diffuse interface model for a smectic phase in contact with an isotropic fluid of different equilibrium densities (e.g. gas with a few sublimated LC molecules), where the smectic is represented by a real-valued order parameter ψ associated with characteristic modulations in the molecular density along the smectic's solid direction. When higher harmonics are negligible, these modulations can be approximately represented by $\psi \approx \frac{1}{2}\left(\bar{A}e^{i\mathbf{q_0}\cdot\mathbf{x}} + \text{c.c.}\right)$, where $\mathbf{q_0}$ is the wave vector in the direction normal to the layers, and $\bar{A}$ is a complex amplitude. The latter has the form $\bar{A} = Ae^{-q_0 u}$, where A is a real amplitude (order

parameter strength) and u represents the displacement away from planar smectic layers. Hence, in this phase-field approach, the smectic is represented by a sinusoidal order parameter, whereas in the isotropic fluid the order parameter is $\psi = 0$ (with amplitude $A = 0$).

The energy $\mathcal{E}$ of the smectic-isotropic system is given by

$$\mathcal{E} = \int_\Omega \left[\rho e + \frac{\zeta}{2}(\rho - \rho_0 - \kappa A)^2\right] d\boldsymbol{x} \,,$$

where e is an energy density per unit mass, ρ is an independent varying density, and ζ is a (finite) constant that controls the penalization magnitude for deviations from the equilibrium density in each phase. This equilibrium density is given by $\rho_0 + \kappa A$, where ρ_0 is the isotropic phase density and κ is a positive constant.

The energy density has the form:

$$e(\psi, \nabla^2\psi) = \frac{1}{2}\left\{\epsilon\,\psi^2 + \alpha[\,(\nabla^2 + q_0^2)\psi\,]^2 - \frac{\beta}{2}\psi^4 + \frac{\gamma}{3}\psi^6\right\},$$

where the $\nabla^2\psi$ dependence makes the energy sensitive to layer distortions and curvatures, allowing this energy to connect with the classic Oseen-Frank description in the limit of small deformations [58]. The control parameter ϵ represents the distance away from the smectic-isotropic transition point, and, alongside the positive constants β and γ, they control the structure of the triple-well energy of the system. Coexistence between the two-phases occurs at $\epsilon_c = 27\beta^2/160\gamma$ (when their energy minima are the same), so that for $\epsilon > \epsilon_c$ the isotropic phase is favored, which can simulate a heat treatment of the LC. Finally, α is a positive constant connected to the splay modulus K_1.

Derivation steps, including nondimensionalization of equations, can be found in Ref. [57]. The resulting governing equations are the balance of mass, balance of linear momentum, and the order parameter equation, where the independent variables are the density ρ, the fluid velocity $\mathbf{v}$, and the order parameter ψ. By denoting the material time derivative as $\dot{(\,)} = \partial_t(\,) + \mathbf{v}\cdot\nabla(\,)$, the system of governing equations is

$$\dot{\rho} = -\rho\nabla\cdot\mathbf{v}\,, \tag{1}$$

$$\begin{aligned}\mathbf{0} = &-\frac{\zeta}{2}\nabla[\rho^2 - (\rho_0 + \kappa A)^2] \\ &+\bar{\mu}\nabla\psi - \rho\nabla e + \eta\nabla^2\mathbf{v} + (\eta + \lambda)\nabla(\nabla\cdot\mathbf{v})\,,\end{aligned} \tag{2}$$

$$\dot{\psi} = -\Gamma\mu\,. \tag{3}$$

Note that the balance of linear momentum takes the form of a Stokes flow, since we assume that inertia is small when compared to viscous effects. In Eq. (2), η and λ are the first and second coefficient of viscosity, respectively (the full viscosity tensor is simplified to the one of a Newtonian fluid), and in Eq. (3) Γ is a mobility constant. The chemical potential μ is given by

$$\begin{aligned}\mu = \frac{\delta\mathcal{E}}{\delta\psi} = &-\kappa\zeta(\rho - \rho_0 - \kappa A)\frac{\psi}{A} + \kappa\zeta q_0^{-2}\nabla\cdot\left[(\rho - \rho_0 - \kappa A)\frac{\nabla\psi}{A}\right] \\ &+ \rho[\epsilon\psi + \alpha q_0^2(\nabla^2 + q_0^2)\psi - \beta\psi^3 + \gamma\psi^5] \\ &+ \alpha\nabla^2[\rho(\nabla^2 + q_0^2)\psi]\,,\end{aligned}$$

and the modified chemical potential $\bar{\mu}$ in Eq. (2) is equal to the last two terms of the previous μ expression.

After setting an initial ψ configuration for the smectic, we integrate the governing equations (1)-(3) numerically through a pseudo-spectral method in three spatial dimensions. We use Neumann boundary conditions for the order parameter, and zero normal fluid velocity on the boundary,

$$\nabla\psi(\mathbf{x})\cdot\hat{\mathbf{N}} = \nabla\nabla^2\psi(\mathbf{x})\cdot\hat{\mathbf{N}} = 0, \quad \mathbf{v}(\mathbf{x})\cdot\hat{\mathbf{N}} = 0, \quad \mathbf{x}\in\partial\Omega\,,$$

where $\hat{\mathbf{N}}$ is the unit normal to the boundary $\partial\Omega$**.** Both Discrete Cosine Transform and Discrete Sine Transform were employed to accommodate these conditions. Due to the Neumann boundary conditions, the smectic layers become perpendicular to the boundaries, connecting to the planar anchoring of molecules on a substrate or walls of a channel. A regular cubic grid is used with linear spacing $\Delta x = 2\pi/n_w q_0$, where n_w is the number of grid points per base smectic wavelength. In our simulations, we employ $n_w = 8$ and $q_0 = 1$, so that $\Delta x = 0.7854$. Further details about numerical integration, amplitude computation, filtering and verification can be found in Refs. [59] and [57]. The developed custom C++ code is publicly available, *smaiso-wcomp*[60], which is based on the parallel FFTW library and the standard MPI passing interface for parallelization.

Previously, numerical results for this model have captured transitions from an initial focal conic configuration towards conical pyramids[57, 58], and concentric rings when simulating a heat treatment, similarly to experiments[15]. While the wave number q_0 was originally associated with modulations across individual layers, another characteristic modulation scale is that of the hemi-cylinders, which are packets of smectic layers whose diameter is of the order $100\ nm$, as observed from SEM images (see Fig. 5). This association leads to a good agreement between the experimental and numerical scale. For example, an initial order parameter configuration consisting of a focal conic with 36 ψ layers would correspond to a TFCD of radius $3.6 - 36\ \mu m$. Another aspect of the model is how it ties surface tension to the splay modulus through its parameters. For small deformations, the splay modulus is given by[58] $K_1 \approx \frac{1}{2}\alpha q_0^2 A^2$. The surface tension can be calculated from $\sigma_H = 4\alpha q_0^2\int_{-\infty}^{\infty}\rho\left(\partial_n A_p\right)^2 dn$, where *n* is the normal coordinate to the interface and A_p is the real amplitude solution across the smectic-isotropic interface. Since $\sigma_H \approx 4\alpha q_0^2 A^2/w$, where $w \approx 2\sqrt{40\alpha\gamma\, q_0^2/27\beta^2}$ is the interface thickness, we approximately have $\sigma_H \approx 8K_1/w$.

For the simulations, we set $\alpha = 1, \beta = 2,\ \gamma = 1$ and $q_0 = 1$, so that if half the wavelength $2\pi/q_0$ is of the order $100\ nm$, then $w \approx 40 - 400$ nm. For a typical smectic A splay modulus value of $K_1 = 30\ pN/m$, the corresponding surface tension is

$\sigma_H \approx 0.6 - 6\ mN/m$. Since the surface tension in smectic free-standing films[61] lies in the range of $10 - 25\ mN/m$ for moderate temperatures $T \lesssim 100°C$, the adopted model parameters set the ration between splay modulus and surface tension to a physically reasonable order, particularly under higher temperatures. The density penalization parameter is kept small $\zeta = 10^{-3}$ when heating the smectic ($\epsilon > \epsilon_c$); larger values of ζ can play a role in changing the effective control parameter and surface tension, and sublimation may come to a halt[57]. Both viscosity constants η and λ are set to 10^3, and the mobility to $\Gamma = 1$. Further, we set $\rho_0 = 10^{-2}$ and $\kappa = 0.813$, so that the equilibrium smectic density is $\rho_s = 1$. Hence, the isotropic phase is a fluid with just a small initial number of LC molecules.

Figure 4 depicts numerical results of the sublimation process of TFCD droplets, limited to circular or elliptical patterns. The differentiation of smectic layer stacks is represented by the red and blue laminae (sinusoidal order parameter ψ), and the isotropic phase is shown in green ($\psi = 0$). The top-view images display the layers on the substrate surface where the torus droplets are located, with thick blue lines indicating the center circle of the tori, and the side-views reveal a center cross-section of the tori. The first case presents an initial order parameter ψ configuration of a half spindle torus, with a focal conic at its center, using a grid of $N = 512^2 \times 256$. The focal conic radius is $a = 100$, and the starting number of ψ layers is 32. When increasing the control parameter to $\epsilon = 0.85 > \epsilon_c = 0.675$ to simulate a heat treatment, we observe that the smetcic gradually sublimates into a small ring torus like configuration. The asymmetry in the interface evolution between the outer and inner part of the torus occurs because of the difference in mean curvature, particularly due to its change in sign close to the focal conic core.

The second set of simulation results in Fig. 4 simulates a TFCD on an elliptical pillar, with an initial condition that mixes stretching and compression of layers with respect to the previous axisymmetric initial condition: the focal conic initial x-direction is stretched by 6.2/5.5 ($N_x = 578$), and the y-direction compressed by 5.2/5.5 ($N_y = 484$). For $\epsilon = 0.85$, besides the interface evolution taking place on top of the torus, we observe that layers close to the bottom slowly become unstable and disappear so that a residual ring torus is not formed. The instability magnifies in the third case, where we stretch the initial layers by 7/5.5 in the x-direction ($N_x = 652$) and compress by 3.4/5.5 in the y-direction ($N_y = 316$).

For elliptical droplets, the asymmetric and pronounced sublimation at the high curvature regions lead to an imbalance and structural deformation. Isotropic liquids, such as water and alcohol, which have relatively high fluidity, can easily alleviate this imbalance through the free flow of the fluid. However, for the smectic A phase and other viscous, anisotropic materials, this structural stress remains unresolved, leading to an irregular phase transition that complicates the prediction of intermediate processes. Partial imbalances in the smectic A phase, and other viscous, and anisotropic materials can lead to the structure's collapse, resulting in irregular and amorphous residues forming. (Fig. 3b and Fig. S5) This behavior highlights the intricate nature of the sublimation process in these materials, where the interplay between structural stress, phase transitions, and surface morphology becomes highly complex.

Smectic Residual 3D Lithography. Lastly, we investigated the thermally sublimed patterns that occur when a TFCD array is formed over a microchannel based on the mechanism forming the hemicylindrical circular residuals that survive relatively longer. When TFCDs are formed within confined channels, their size and arrangement can be varied according to the depth and width of the channels. For example, when the Y002 is filled in microchannels of width 5 and depth 5 μm, the arrays of TFCDs show a linear pattern (Fig. S8), in which each array is independent of the other. However, when the TFCD film is formed thicker than the height of the channel, the arrangement of TFCDs, formed through planar anchoring-based epitaxial self-assembly of SmA LC molecules along the channel's terrain, can exhibit its typical hexagonal array by connecting the smectic layers in TFCDs (Fig. 5a). In the microchannel, the centers of TFCDs are positioned along its main direction and arranged in a staggered manner with respect to adjacent channels, resulting in the formation of a hexagonal array over the channels.

Interestingly, as shown in SEM images (Fig. 5b) and the corresponding schematic sketches (Fig. 5c), the annealed structures of the TFCDs in the channel are considerably different from that of TFCDs on a flat substrate (Fig. 1c and Fig. S3), in which the hemicylindrical patterns is seemingly elongated perpendicular to the channel while the concentric patterns of the hemicylinders are revealed on the flat substrate. Focusing on a single TFCD in the channel, it initially exhibits concentric patterns of the hemicylinders, which are highly similar to the patterns on a flat substrate. With further annealing, the hemicylinders are seemingly transformed into elongated patterns across the width of the channel (Fig. 5d).

Simulation results clearly depict the corresponding topographical evolution of annealed TFCDs confined in the channel, as observed through the modulation evolution of the hemicylinders on the bottom of the channel (Fig. 5e). These simulations use a grid of $N = 256 \times 128 \times 256$, and an initial order parameter configuration consisting of a TFCD similar to the ones in experiments (Fig. 5d), whose film depth is higher than the channel's height. Both the channel walls and the substrate present a neighborhood favoring the smectic and planar anchoring, to connect with the surface treatment of the substrate in experiments. As in the previous section, we use $\epsilon = 0.85 > \epsilon_c = 0.675$ in the numerical experiments to simulate the annealing. We observe that the bottom layers restructure, favoring hemicylinders that are perpendicular to the walls, which are later exposed as the outer layers continue to sublime.

The formation of a hemispherical cylinder structure in experiments is due to the partial rearrangement of Y002 molecules normal to the air interface, during the sublimation process of Y002 on the surface of TFCDs.[43] Therefore, the molecular alignment within the internal layers is consistently perpendicular to the long axis of the hemispherical cylinder. Based on this fact, by examining the intermediate structures that result from the layer-by-layer evaporation during the sublimation process, the layered structure and molecular alignment within the initial TFCDs can be sequentially confirmed

throughout its thickness. Thus, as observed with TFCDs' thermal annealing process on flat substrates and as inferred from the Maltese cross pattern of TFCDs observed through polarized optical microscopy (POM), it can be inferred that on flat substrates, molecular alignment at the bottom surface occurs radially with a defect-centered orientation. However, in the case of TFCDs on channel substrates, while POM images might not clearly distinguish them from those on flat substrates, SEM images of structures processed at 160 ℃ for 40 minutes reveal that the molecular alignment at the bottom of the channel is parallel to the long axis of channels (4th image in Fig. 5d), distinct from the radial orientation (Fig. S4). The above results introduce a new method for analyzing the internal structure of smectic LCs, which can complement the limitations of observation on layered LC structures using POM. Furthermore, it holds potential as a novel fabrication technique capable of hierarchically forming micro-nanostructures on the surface of three-dimensional structures.

Conclusions

In conclusion, our study has demonstrated the precise spatial control achieved by depositing smectic LCs on patterned silicon substrates and isolating TFCD in a well-defined arrangement. Sublimation of the LCs was used to indirectly assess the energy properties of the TFCD structures, with the thickness of the LC layer and parameters of the substrate pattern enabling the production of isolated TFCDs. These findings provide us with a greater understanding of the behavior of torus-shape droplets and how the shape of the patterned substrate greatly influences their arrangement. Simulation results indicate that the arrangement of TFCDs is significantly influenced by the shape of the patterned silicon substrate, and a geometric model was proposed to accurately estimate the energy effects of nonzero eccentricity and assess their thermodynamic stability. This model can help us better understand the stability of the TFCD structures, so that geometric parameters of the silicon substrate can be manipulated to produce unique patterns.

Sublimation can be considered as a measure of molecular arrangement stability: the more unstable the state, the faster sublimation occurs. In the elliptical shape, TFCD has a more distorted and unstable structure, thus leading to faster sublimation. Our findings provide valuable insights into the behavior of smectic LCs, and open up new possibilities for the development of novel LC-based devices with precise control over their topological properties. By manipulating the parameters of the silicon substrate, it is possible to create TFCD arrangements that are thermodynamically stable, and therefore less likely to be affected by sublimation. This can be applied to understand and utilize the fine patterning of organic molecules in various applications such as photonic devices, nano sensors, and more.

Author Contributions

W.K., E.V., P.L., J.V., D.S.K., D.K.Y. designed research. W.K., E.V. performed research. W.K., E.V., P.L., J.V., D.S.K., D.K.Y. wrote the paper.

Conflicts of interest

The authors declare no competing interest.

Acknowledgements

This was supported by the KAIST Grand Challenge 30 Project (KC30) and the National Research Foundation (NRF) funded by the Korean Government (MSIT) (RS-2023-00273025 and 2021R1F1A1047516). This research was also supported by the Extreme Science and Engineering Discovery Environment (XSEDE), which is supported by the National Science Foundation under Grant No. ACI-1548562.

Notes and references

1. Zuo, X.B., *Structural Studies on Soft Matter Self-Assembly with Small-Angle X-ray Scattering.* Acta Crystallographica a-Foundation and Advances, 2021. **77**: p. A204-A204.
2. Stupp, S.I., et al., *Self-assembly of biomolecular soft matter.* Faraday Discuss, 2013. **166**: p. 9-30.
3. Sagar, G.H., M.A. Arunagirinathan, and J.R. Bellare, *Self-assembled surfactant nano-structures important in drug delivery: A review.* Indian Journal of Experimental Biology, 2007. **45**(2): p. 133-159.
4. Viswanathan, P., et al., *Monolayer assembly of gold nanodots on polyelectrolyte support: A multifunctional electrocatalyst for reduction of oxygen and oxidation of sulfite and nitrite.* Bulletin of the Korean Chemical Society, 2022. **43**(3): p. 396-401.
5. Zhu, W.K., et al., *Self-assembly of covalent porphyrin compound and its enhanced electrochemiluminescence performance.* Bulletin of the Korean Chemical Society, 2022. **43**(12): p. 1373-1382.
6. Pezzutti, A.D., L.R. Gómez, and D.A. Vega, *Smectic block copolymer thin films on corrugated substrates.* Soft Matter, 2015. **11**(14): p. 2866-2873.
7. Diaz, J., et al., *Nematic Ordering of Anisotropic Nanoparticles in Block Copolymers.* Advanced Theory and Simulations, 2022. **5**(1).
8. Beales, P.A., et al., *Reversible Assembly of Stacked Membrane Nanodiscs with Reduced Dimensionality and Variable Periodicity.* Journal of the American Chemical Society, 2013. **135**(9): p. 3335-3338.
9. Noguchi, H. and J.B. Fournier, *Membrane structure formation induced by two types of banana-shaped proteins.* Soft Matter, 2017. **13**(22): p. 4099-4111.
10. Lee, H., et al., *Binding Energy-dependent Growth Behaviors and Surface Characteristics of Sequentially Polymerized Zincone Films.* Bulletin of the Korean Chemical Society, 2020. **41**(1): p. 54-59.
11. Yoon, D.K., et al., *Three-dimensional textures and defects of soft material layering revealed by thermal sublimation.* Proceedings of the National Academy of Sciences of the United States of America, 2013. **110**(48): p. 19263-19267.
12. Hochbaum, A., *Thermally Addressed Smectic Liquid-Crystal Displays.* Optical Engineering, 1984. **23**(3): p. 253-260.
13. Honglawan, A., et al., *Synergistic assembly of nanoparticles in smectic liquid crystals.* Soft Matter, 2015. **11**(37): p. 7367-7375.

14. Kim, D.S., et al., *Grooving of nanoparticles using sublimable liquid crystal for transparent omniphobic surface.* Journal of Colloid and Interface Science, 2018. **513**: p. 585-591.
15. Kim, D.S., et al., *Controlling Gaussian and mean curvatures at microscale by sublimation and condensation of smectic liquid crystals.* Nature Communications, 2016. **7**.
16. Hare, S.M., et al., *Chiral Liquid Crystal Lenses Confined in Microchannels.* Materials, 2020. **13**(17).
17. Barois, P., et al., *Application of X-ray resonant diffraction to structural studies of liquid crystals.* European Physical Journal-Special Topics, 2012. **208**(1): p. 333-350.
18. Ostrovskiĭ, B.I., *X-ray diffraction study of nematic, smectic A and C liquid crystals*. Soviet scientific reviews. Section A, physics reviews vol. 12, part 2. 1989, Chur: Harwood Academic.
19. Hazelwood, L.D., *Theories of defect structures found in smectic-A liquid crystals*. 1998: Original typescript. 165p.
20. Alsuhaimi, O.A., et al., *Stability and instability of planar layers of smectic A liquid crystals*. 2021, Great Britain: University of Dundee.
21. Stewart, F. and S. University of, *The mathematical modelling of dynamics in smectic A liquid crystals*. 2008, Glasgow: University of Strathclyde.
22. Chen, H.Y. and D. Jasnow, *Layer dynamics of freely standing smectic-A films.* Physical Review E, 2000. **61**(1): p. 493-503.
23. Filimonova, E.S., A.V. Emel'yanenko, and J.H. Liu, *A Study of Polarization in Smectic Liquid Crystals via Statistical-Physics Methods.* Moscow University Physics Bulletin, 2017. **72**(4): p. 369-375.
24. Sliwa, I. and A.V. Zakharov, *Structural, Optical and Dynamic Properties of Thin Smectic Films.* Crystals, 2020. **10**(4).
25. Pieranski, P., et al., *Physics of Smectic Membranes.* Physica A, 1993. **194**(1-4): p. 364-389.
26. Bramble, J.P., et al., *Observations of focal conic domains in smectic liquid crystals aligned on patterned self-assembled monolayers.* Liquid Crystals, 2007. **34**(10): p. 1137-1143.
27. Kim, Y.H., et al., *Confined Self-Assembly of Toric Focal Conic Domains (The Effects of Confined Geometry on the Feature Size of Toric Focal Conic Domains).* Langmuir, 2009. **25**(3): p. 1685-1691.
28. Honglawan, A., et al., *Pillar-Assisted Epitaxial Assembly of Toric Focal Conic Domains of Smectic-A Liquid Crystals.* Advanced Materials, 2011. **23**(46): p. 5519-+.
29. Fujii, S., et al., *Elasticity of smectic liquid crystals with focal conic domains.* Journal of Physics-Condensed Matter, 2011. **23**(23).
30. Yoon, D.K., et al., *Internal structure visualization and lithographic use of periodic toroidal holes in liquid crystals.* Nature Materials, 2007. **6**(11): p. 866-870.
31. Baliyan, V.K., S.H. Lee, and S.W. Kang, *Optically and spatially templated polymer architectures formed by photopolymerization of reactive mesogens in periodically deformed liquid crystals.* Npg Asia Materials, 2017. **9**.
32. Gharbi, I., et al., *Persistence of Smectic-A Oily Streaks into the Nematic Phase by UV Irradiation of Reactive Mesogens.* Crystals, 2017. **7**(12).
33. Honglawan, A., et al., *Topographically induced hierarchical assembly and geometrical transformation of focal conic domain arrays in smectic liquid crystals.* Proceedings of the National Academy of Sciences of the United States of America, 2013. **110**(1): p. 34-39.
34. Kim, D.S., et al., *Creation of a superhydrophobic surface from a sublimed smectic liquid crystal.* Rsc Advances, 2014. **4**(51): p. 26946-26950.
35. Zhang, M., et al., *Vapor pressure of nine perfluoroalkyl substances (PFASs) determined using the Knudsen Effusion Method.* J Chem Eng Data, 2020. **65**(5): p. 2332-2342.
36. Barton, C.A., M.A. Botelho, and M.A. Kaiser, *Solid Vapor Pressure and Enthalpy of Sublimation for Ammonium Perfluorooctanoate.* Journal of Chemical and Engineering Data, 2009. **54**(3): p. 752-755.
37. Suh, A., et al., *Controllable liquid crystal defect arrays induced by an in-plane electric field and their lithographic applications.* Journal of Materials Chemistry C, 2019. **7**(6): p. 1713-1719.
38. Shin, M.J., M.J. Gim, and D.K. Yoon, *Directed Self-Assembly of Topological Defects of Liquid Crystals.* Langmuir, 2018. **34**(7): p. 2551-2556.
39. Rosenblatt, C. and N.M. Amer, *Optical Determination of Smectic a Layer Spacing in Freely Suspended Thin-Films.* Bulletin of the American Physical Society, 1980. **25**(3): p. 213-213.
40. Haldar, S., et al., *Smectic Layer Spacing, Average Intermolecular Distance and Spontaneous Polarization of Room Temperature FLC Mixtures.* Molecular Crystals and Liquid Crystals, 2011. **547**: p. 25-32.
41. Allender, D. and M. Kuzma, *Self-Consistent Treatment of the Layer Spacing in Smectic a Liquid-Crystals.* Bulletin of the American Physical Society, 1979. **24**(3): p. 250-251.
42. Lavrentovich, O.D., M. Kleman, and V.M. Pergamenshchik, *Nucleation of Focal Conic Domains in Smectic-a Liquid-Crystals.* Journal De Physique Ii, 1994. **4**(2): p. 377-404.
43. Designolle, V., et al., *AFM study of defect-induced depressions of the smectic-A/air interface.* Langmuir, 2006. **22**(1): p. 363-368.
44. Guo, W. and C. Bahr, *Influence of anchoring strength on focal conic domains in smectic films.* Physical Review E, 2009. **79**(1).
45. Kim, D.S., et al., *Arrangement and SERS Applications of Nanoparticle Clusters Using Liquid Crystalline Template.* Acs Applied Materials & Interfaces, 2017. **9**(8): p. 7787-7792.
46. Ma, L.L., et al., *Smectic Layer Origami via Preprogrammed Photoalignment.* Advanced Materials, 2017. **29**(15).
47. Blank, M., P. Nair, and T. Poschel, *Modeling surface tension in Smoothed Particle Hydrodynamics using Young-Laplace pressure boundary condition.* Computer Methods in Applied Mechanics and Engineering, 2023. **406**.
48. Wan, H.L., et al., *Interface Wetting Driven by Laplace Pressure on Multiscale Topographies and Its Application to Performance Enhancement of Metal-Composite Hybrid Structure.* Acs Applied Materials & Interfaces, 2023. **15**(14): p. 18427-18439.
49. Svintradze, D.V., *Generalization of Young-Laplace, Kelvin, and Gibbs-Thomson equations for arbitrarily curved surfaces.* Biophysical Journal, 2023. **122**(5): p. 892-904.
50. Syms, R.R.A., et al., *Surface tension-powered self-assembly of micro structures - The state-of-the-art.* Journal of Microelectromechanical Systems, 2003. **12**(4): p. 387-417.
51. Timm, M.L., et al., *Evaporation of a sessile droplet on a*

slope. Scientific Reports, 2019. **9**.
52. Fragkopoulos, A.A., et al., *Toroidal Droplets: Growth Rates, Dispersion Relations, and Behavior in the Thick-Torus Limit.* Langmuir, 2018. **34**(3): p. 1218-1224.
53. Fragkopoulos, A.A., et al., *Shrinking instability of toroidal droplets.* Proceedings of the National Academy of Sciences of the United States of America, 2017. **114**(11): p. 2871-2875.
54. Heinzen, C., et al., *Use of vibration technology for jet break-up for encapsulation of cells, microbes and liquids in monodisperse microcapsules.* Practical Aspects of Encapsulation Technologies, 2002: p. 19-25.
55. Gibbs, J.W., *The collected works of J. Willard Gibbs*. 1928, New York ; London: Longmans, Green & Co.
56. Gennes, P.-G.d., et al., *Capillarity and wetting phenomena : drops, bubbles, pearls, waves*. 1st ed. 2004, New York, NY: Springer New York.
57. Vitral, E., P.H. Leo, and J. Vinals, *Phase-field model for a weakly compressible soft layered material: morphological transitions on smectic-isotropic interfaces.* Soft Matter, 2021. **17**(25): p. 6140-6159.
58. Vitral, E., P.H. Leo, and J. Vinals, *Role of Gaussian curvature on local equilibrium and dynamics of smectic-isotropic interfaces.* Physical Review E, 2019. **100**(3).
59. Vitral, E., P.H. Leo, and J. Vinals, *Model of the dynamics of an interface between a smectic phase and an isotropic phase of different density.* Physical Review Fluids, 2020. **5**(7).
60. Vitral, E., *smaiso-wcomp: weakly compressible smectic-isotropic system.* Zenodo, 2021: p. v1.0.0.
61. Mach, P., et al., *Surface tension obtained from various smectic free-standing films: The molecular origin of surface tension.* Langmuir, 1998. **14**(15): p. 4330-4341.